Microscopic analysis of ^{11}Li elastic scattering on protons and breakup processes within the ^{9}Li + 2n cluster model

V. K. Lukyanov,[1] D. N. Kadrev,[2] E. V. Zemlyanaya,[1] A. N. Antonov,[2] K. V. Lukyanov,[1] M. K. Gaidarov,[2,*] and K. Spasova[2,3]

[1]*Joint Institute for Nuclear Research, Dubna 141980, Russia*

[2]*Institute for Nuclear Research and Nuclear Energy, Bulgarian Academy of Sciences, Sofia 1784, Bulgaria*

[3]*University "Ep. K. Preslavski," Shumen 9712, Bulgaria*

(Received 27 May 2013; revised manuscript received 22 July 2013; published 27 September 2013)

In the paper, the results of analysis of elastic scattering and breakup processes in interactions of the ^{11}Li nucleus with protons are presented. The hybrid model of the microscopic optical potential (OP) is applied. This OP includes the single-folding real part, while its imaginary part is derived within the high-energy approximation theory. For ^{11}Li + p elastic scattering, the microscopic large-scale shell model (LSSM) density of ^{11}Li is used. The depths of the real and imaginary parts of the OP are fitted to the elastic scattering data at 62, 68.4, and 75 MeV/nucleon, being simultaneously adjusted to reproduce the true energy dependence of the corresponding volume integrals. The role of the spin-orbit potential is studied and predictions for the total reaction cross sections are made. Also, the cluster model, in which ^{11}Li consists of a 2n-halo and the ^{9}Li core having its own LSSM form of density, is adopted. The respective microscopic proton-cluster OPs are calculated and folded with the density probability of the relative motion of both clusters to get the whole ^{11}Li + p OP. The breakup cross sections of ^{11}Li at 62 MeV/nucleon and momentum distributions of the cluster fragments are calculated. An analysis of the single-particle density of ^{11}Li within the same cluster model accounting for the possible geometric forms of the halo-cluster density distribution is performed.

DOI: 10.1103/PhysRevC.88.034612 PACS number(s): 24.10.Ht, 25.40.Cm, 25.60.Gc, 21.10.Gv

I. INTRODUCTION

Recent experiments with radioactive ion beams have opened a new era in nuclear physics by providing the possibility to study light nuclei far from stability. Indeed, the availability of radioactive ion beams favored the discovery of halo nuclei [1]. A typical example is the neutron halo in the nucleus ^{11}Li, revealed as a consequence of its very large interaction radius, deduced from the measured interaction cross sections of ^{11}Li with various target nuclei [2–4]. The halo of the nucleus extends its matter distribution to a large radius. A hypothesis based on early data [2] on the important role played by neutron pairing for the stability of nuclei near the drip line is suggested in Refs. [5] and [6], and in particular, the direct link of the matter radius to the 2n weak binding in ^{11}Li is claimed to be attributed to its configuration as a ^{9}Li core coupled to a dineutron.

The experiments that provide evidence of the existence of a halo in this nucleus are related not only to measurements of the total-reaction cross section for ^{11}Li projectiles but also to the momentum distributions of the ^{9}Li or neutron fragments following the breakup of ^{11}Li at high energies [7–10], e.g., the process ^{11}Li +^{12}C at E = 800 MeV/nucleon in Ref. [7]. Here we mention also the experiments at lower energies, E = 60 MeV/nucleon, of scattering of ^{11}Li on ^{9}Be, ^{93}Nb, and ^{181}Ta in [11] and of ^{11}Li in a wide range of nuclei, from ^{9}Be to ^{238}U in [12]. It was shown that the momentum distribution of the breakup fragments has a narrow peak, much narrower than that observed in the fragmentation of well-bound nuclei. This property has been interpreted (e.g., [13–19]) as being related to the very large extension of the wave function, compared to that of the core nucleus, leading to the existence of the nuclear halo. As pointed out in Ref. [17], the longitudinal component of the momentum (taken along the beam or z direction) gives the most accurate information on the intrinsic properties of the halo and is insensitive to details of the collision and the size of the target.

The differential cross sections for small-angle proton elastic scattering on Li isotopes at energies near 700 MeV/nucleon were measured in inverse kinematics with secondary nuclear beams at GSI (Darmstadt) [20]. They have been analyzed using the Glauber theory and information on the nuclear matter density distributions has been extracted. It was supposed that the two valence neutrons in ^{11}Li, which form the halo, could move in a wide region far from the ^{9}Li core that is related to the low two-neutron separation energy (∼0.3 MeV).

The idea of the existence of a two-neutron halo in ^{11}Li was experimentally verified in measurements and studies of differential cross sections of ^{11}Li + p elastic scattering in the energy range 60–75 MeV/nucleon [21–23]. The data analysis at 62 MeV/nucleon [21] showed that the adjusted phenomenological Woods-Saxon (WS) potential has a shallow real part and an imaginary part with a long tail. In Refs. [22] and [23] the data at 65–75 MeV/nucleon were analyzed using the parameter-free cluster-orbital shell-model approximation (COSMA) [24] and a conclusion was drawn that ^{11}Li + p scattering is mainly determined by scattering on the ^{9}Li core. In various work (e.g., Refs. [25–29]) the calculations of the ^{11}Li + p differential cross sections in the energy range E < 100 MeV/nucleon differ among themselves by the assumptions on how the ^{11}Li + p optical potential (OP) should be constructed. Most of them use the simple folding approach to the real part of the OP (ReOP) without accounting for the

*gaidarov@inrne.bas.bg

exchange terms and with the introduction of different forms of effective nucleon-nucleon (*NN*) interactions. To calculate the folding potentials, the constituent $^{9}\mathrm{Li}+2n$ cluster model was usually employed, in which the ^{11}Li density has two separated parts taken in explicit forms. Various suggestions were made for the imaginary part of the OP (ImOP) like the WS and Gaussian forms or calculated within the t-matrix method. Then the cross sections were computed numerically by using the eikonal approximation or starting with the Glauber multiple scattering theory. The more complicated model of ^{11}Li treated as a $^{9}\mathrm{Li}+n+n$ three-body system was developed in Ref. [30], where the effects of the halo distribution in ^{11}Li in correspondence to different parts of the three-body wave function are manifested in the elastic cross section.

Generally, here we would like to outline the advantages of the microscopic analyses using the coordinate-space g-matrix folding method (e.g., Ref. [31]) as well as work (e.g., Ref. [32]) where the ReOP is microscopically calculated using effective *NN* interactions within a folding approach [33–36] and including also the exchange terms in it. In recent works [37,38] the $^{11}\mathrm{Li}+p$ elastic scattering cross sections were analyzed using the folding procedure and effective *NN* forces to calculate the ReOP taking into account only its direct part and not the exchange one. In Ref. [37] the volume ImOP was taken either in a WS form or in the form of the direct folded ReOP, and in Ref. [38] an application of the microscopic OP [39,40] developed on the basis of the high-energy approximation (HEA) theory [41,42] was also made. To this end, phenomenological densities (Gaussian types and COSMA) have been used in the calculations [37] and the large-scale shell-model (LSSM) densities of ^{9,11}Li [43] in Ref. [38] as well.

The aims of our work are as follows. First, we study elastic scattering cross sections for $^{11}\mathrm{Li}+p$ at three incident energies ($E<100$ MeV/nucleon) using microscopically calculated OPs within the hybrid model [39]. The ReOP includes the direct and exchange terms and the ImOP is based on the HEA. We follow our previous work [44–46], where this model was applied to elastic scattering of the exotic nuclei ^{6,8}He with the use of their LSSM densities, thus avoiding an adjustment of free parameters. As in Ref. [45], we pay attention to the ambiguity problem when fitting the coefficients Ns that renormalize the strengths of different parts of the OP. This ambiguity is minimized in Ref. [47] by testing the condition that the true energy dependence of the volume integrals must fulfill. Second, in addition to the analysis of elastic scattering cross sections, we estimate other characteristics of the reaction mechanism such as the ^{11}Li total-reaction and breakup cross sections. The theoretical scheme used in this second part of the work is based on the procedure from the first part to calculate microscopically the potentials necessary for the evaluation of the other quantities within the model. The calculations are performed by using the $^{11}\mathrm{Li}+p$ OP constructed as a sum of the microscopically calculated OP of $^{9}\mathrm{Li}+p$ and the $(2n\text{-halo})+p$ potential folded with a density probability of the relative motion of clusters. For a more consistent description of the halo structure of ^{11}Li we calculate the fragment momentum distributions from $^{11}\mathrm{Li}+p$ reaction at 62 MeV/nucleon within the same breakup reaction model and present predictions for them. Finally, we give results for the single-particle density distribution of ^{11}Li within the true two-cluster model considering the relative motion of clusters ($^{9}\mathrm{Li}+h$) that is ensured by the respective wave function and make a comparison with other calculations.

The structure of this article is as follows. The theoretical scheme to calculate microscopically the ReOP, ImOP, and spin-orbit term, as well as the results of the calculations of the elastic scattering of ^{11}Li on protons and the discussion, is given in Sec. II. Section III reports the basic expressions to estimate the ^{11}Li breakup and to calculate the momentum distributions of its products. The same section contains the results of the total breakup cross sections, the momentum distributions of clusters, and the single-particle density distribution of ^{11}Li calculated within the breakup model of ^{11}Li. A summary and the conclusions of the work are given in Sec. IV.

II. ELASTIC SCATTERING OF ^{11}Li ON PROTONS AT $E<100$ MeV/NUCLEON

A. Microscopic ReOP

The OP used in our calculations has the form

$$U_{\mathrm{opt}}=V^{F}(r)+iW(r). \tag{1}$$

In Sec. II C we also add a spin-orbit term to U_{opt} from Eq. (1).

The real part of the nucleon-nucleus OP is assumed to be the result of a folding of the nuclear density and of the effective *NN* potential and involves the direct and exchange parts (e.g., Refs. [33–35]; see also [44] and [45]):

$$V^{F}(r)=V^{D}(r)+V^{\mathrm{EX}}(r). \tag{2}$$

The direct part $V^{D}(r)$ is composed of the isoscalar (IS) and isovector (IV) contributions,

$$V^{D}_{\mathrm{IS}}(r)=\int\rho_2(\mathbf{r}_2)g(E)F(\rho_2)v^{D}_{00}(s)d\mathbf{r}_2, \tag{3}$$

$$V^{D}_{\mathrm{IV}}(r)=\int\delta\rho_2(\mathbf{r}_2)g(E)F(\rho_2)v^{D}_{01}(s)d\mathbf{r}_2, \tag{4}$$

with $\mathbf{s}=\mathbf{r}+\mathbf{r}_2$, and

$$\rho_2(\mathbf{r}_2)=\rho_{2,p}(\mathbf{r}_{2,p})+\rho_{2,n}(\mathbf{r}_{2,n}), \tag{5}$$

$$\delta\rho_2(\mathbf{r}_2)=\rho_{2,p}(\mathbf{r}_{2,p})-\rho_{2,n}(\mathbf{r}_{2,n}). \tag{6}$$

In Eqs. (5) and (6), $\rho_{2,p}(\mathbf{r}_{2,p})$ and $\rho_{2,n}(\mathbf{r}_{2,n})$ are the proton and neutron densities of the target nucleus. The expressions for the energy and density dependence of the effective *NN* interaction [the formulas for $g(E)$ and $F(\rho)$] are given, e.g., in Ref. [45]. For the *NN* potentials v^{D}_{00} and v^{D}_{01} we use the expression from Ref. [35] for the CDM3Y6 type of effective interaction based on the Paris *NN* potential. The IS part of the exchange contribution to the ReOP has the form

$$V^{\mathrm{EX}}_{\mathrm{IS}}(r)=g(E)\int\rho_2(\mathbf{r}_2,\mathbf{r}_2-\mathbf{s})F(\rho_2(\mathbf{r}_2-\mathbf{s}/2))\times v^{\mathrm{EX}}_{00}(s)j_0(k(r)s)d\mathbf{r}_2, \tag{7}$$

ρ_2 being the one-body density matrix. It is shown in Ref. [44] how the IV part of the exchange ReOP can be obtained. Here

we would like to emphasize the general importance of the account for the exchange part of the OP. As shown in different examples in Ref. [35], the exchange effects lead, for instance, to a particular energy dependence of the total potential and to different signs of the direct and exchange inelastic form factors and others, so they should be treated as accurately as possible.

The LSSM proton and neutron densities used in our work for ^{11}Li are calculated in a complex $2\hbar\omega$ shell-model space using the WS basis of single-particle wave functions with exponential asymptotic behavior [43], which is, in principle, the realistic one. Here we would like to discuss this point. In many works, to simplify analytical studies and calculations one uses basic functions and densities with Gaussian asymptotics of the type $\exp(-ar^2)$, while it has to be the exponential one, $\exp(-br)/r$, where parameter b is related to the bound energy of the particle in the upper shell. This difference can affect the results for cross sections in the region of relatively large angles of scattering. This point was one of the reasons the LSSM densities [43] for ^{9,11}Li were used in our work.

B. Optical potential within the high-energy approximation

In the present work we use the hybrid model of the OP [39], in which its imaginary part was derived within the HEA theory [41,42], while the real part is obtained as prescribed by the folding procedure in Sec. II A. The cross sections are calculated by means of the DWUCK4 code [48] for solving the Schrödinger equation. To obtain the HEA OP one can use the definition of the eikonal phase as an integral of the nucleon-nucleus potential over the trajectory of the straight-line propagation, and one has to compare it with the corresponding Glauber expression for the phase in the optical limit approximation. In this way, the HEA OP is obtained as a folding of the form factors of the nuclear density and the NN amplitude $f_{NN}(q)$ [39,40]:

$$U^H_{\rm opt} = V^H + iW^H = -\frac{\hbar v}{(2\pi)^2}(\bar{\alpha}_{NN}+i)\bar{\sigma}_{NN} \times \int_0^\infty dq q^2 j_0(qr)\rho_2(q) f_{NN}(q). \quad (8)$$

In Eq. (8) $\bar{\sigma}_{NN}$ and $\bar{\alpha}_{NN}$ are, respectively, the NN total scattering cross section and the ratio of the real to the imaginary part of the forward NN scattering amplitude, both averaged over the isospin of the nucleus. These two quantities have been parametrized in [49] and [50] as functions of energies up to 1 GeV. The values of $\bar{\sigma}_{NN}$ and $\bar{\alpha}_{NN}$ can also account for the in-medium effect by a factor from Ref. [51].

C. The spin-orbit term

The expression for the spin-orbit contribution to the OP used in our work is added to the right-hand side of Eq. (1) and has the form

$$V_{\rm LS}(r) = 2\lambda_\pi^2\left[V_0\frac{1}{r}\frac{df_R(r)}{dr} + iW_0\frac{1}{r}\frac{df_I(r)}{dr}\right](\mathbf{l}\cdot\mathbf{s}), \quad (9)$$

where $\lambda_\pi^2 = 2$ fm^2 is the squared pion Compton wavelength, and V_0 and W_0 are the real and imaginary parts of the microscopic OP at $r = 0$. In our work, in Eq. (9) the functions $f_R(r)$ and $f_I(r)$ are taken as WS forms $f(r, R_R, a_R)$ and $f(r, R_I, a_I)$, with the half-radius $R_R(R_I)$ and diffuseness $a_R(a_I)$ parameters obtained by the best fit of the WS potential to the microscopically calculated real $V(r)$ and imaginary $W(r)$ parts of the OP.

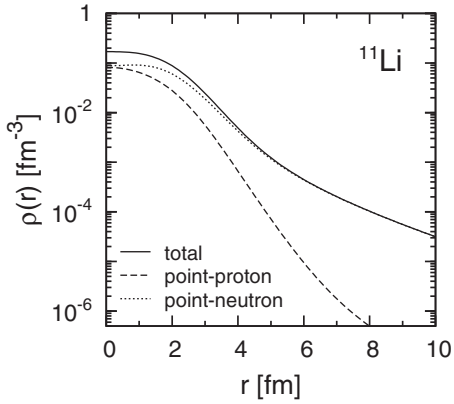

FIG. 1. Total (normalized to $A = 11$), point-proton (normalized to $Z = 3$), and point-neutron (normalized to $N = 8$) densities of ^{11}Li obtained in the LSSM approach [43].

D. Results of calculations of ^{11}Li + p elastic scattering

In the beginning of this subsection we consider ^{11}Li + p elastic scattering at three energies, 62, 68.4, and 75 MeV/nucleon, for which the differential cross sections have been measured [21–23]. The respective folding OPs V^F and W^H are calculated by the procedure described in Secs. II A–II C using Eqs. (1)–(9), and then the whole OP is constructed in the form

$$U_{\rm opt}(r) = N_R V^F(r) + iN_I W(r) + 2\lambda_\pi^2\left\{N_R^{\rm SO}V_0^F\frac{1}{r}\frac{df_R(r)}{dr} + iN_I^{\rm SO}W_0^H\frac{1}{r}\frac{df_I(r)}{dr}\right\}(\mathbf{l}.\mathbf{s}). \quad (10)$$

The OP $U_{\rm opt}(r)$, (10), is applied to calculate the elastic scattering differential cross sections using the program DWUCK4 [48]. The number of partial waves is controlled by the parameter LMAX that corresponds to the maximum partial wave for the distorted waves. We use the parameter LMAX = 100. For the densities of protons and neutrons of ^{11}Li we use the LSSM ones [43] (shown in Fig. 1) that have an exponential asymptotics which is the correct one. As can be seen from Eq. (10), we introduce and consider the set of N coefficients as parameters that can be found by fitting the calculated to the experimental differential cross sections of ^{11}Li + p elastic scattering. Moreover, the fitting procedure can be constrained by additional conditions on the behavior of the OPs (as in Refs. [44–46] and show below). The real and imaginary parts of the SO OP in (10) are approximated by the WS form. Their parameters $V_0^F(W_0^H)$, $R_R(R_I)$, and $a_R(a_I)$ were obtained by a fitting procedure to the respective calculated microscopic potentials $V^F(r)$ and $W^H(r)$. We take the ImOP in two forms, the microscopically obtained W^H within HEA ($W = W^H$) or the form of the folded real potential V^F ($W = V^F$).

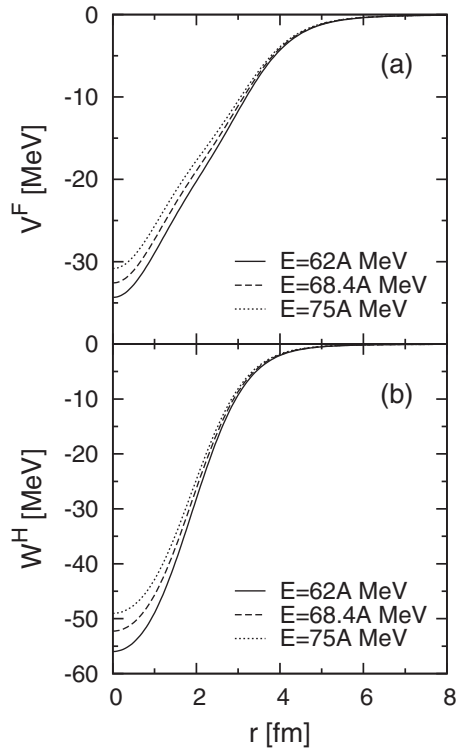

FIG. 2. Microscopic real part (V^F) of the OP (a) and HEA imaginary part (W^H) (b) calculated using the LSSM densities for energies $E = 62$ MeV/nucleon (solid lines), $E = 68.4$ MeV/nucleon (dashed lines), and $E = 75$ MeV/nucleon (dotted lines).

Concerning our approach using the set of N coefficients as parameters we consider it to be the appropriate physical basis, which constrains the fitting procedure by the established model forms of the potentials. We emphasize that in our work we do not aim to find perfect agreement with the experimental data. In this sense, however, the usage of the fitting parameters (N's) related to the depths of the different components of the OPs can be considered as a way to introduce a quantitative measure of the deviations of the predictions of our method (with the account for the exchange contributions to the OP) from the reality (e.g., the differences of N's from unity for given energies, as shown below). Thus, the closeness of the N values to unity could show the ability of the approach to give absolute values of the intensity of the OPs.

The microscopic real part (V^F) of the OP and the HEA imaginary part (W^H) calculated using LSSM densities of ^{11}Li are shown in Fig. 2 for different energies. In Fig. 3 we give as an example the differential cross section of the elastic scattering $^{11}\mathrm{Li} + p$ at 62 MeV/nucleon in cases where $W = W^H$ and $W = V^F$ with and without accounting for the spin-orbit term in Eq. (10). The renormalization parameters N are determined by a fitting procedure. The results of the calculations are close to each other and that is why all of them are shown within shaded areas in Fig. 3. The following definition of χ^2 is used:

$$\chi^2 = \frac{1}{N}\sum_{i=1}^{N}\left[\frac{\sigma^{\mathrm{exp}}(\vartheta_i) - \sigma^{\mathrm{th}}(\vartheta_i)}{\Delta\sigma^{\mathrm{exp}}(\vartheta_i)}\right]^2, \qquad (11)$$

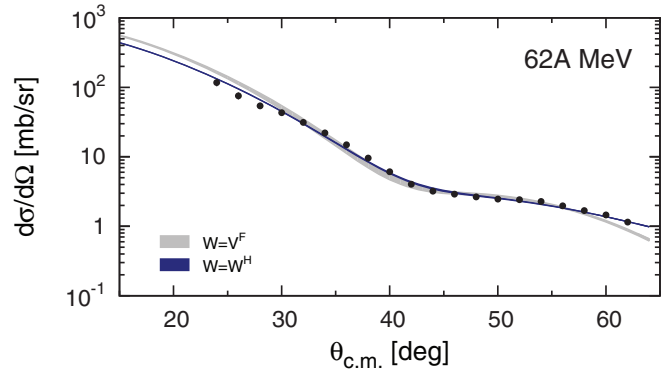

FIG. 3. (Color online) $^{11}\mathrm{Li} + p$ elastic scattering cross section at $E = 62$ MeV/nucleon using U_{opt} [Eq. (10)] for values of the parameters listed in Table I. Darker (blue) area, $W = W^H$; gray area, $W = V^F$. Experimental data are taken from Ref. [21].

where $\sigma^{\mathrm{th}}(\vartheta_i)$ and $\sigma^{\mathrm{exp}}(\vartheta_i)$ are the theoretical and experimental values of the differential cross sections ($d\sigma/d\Omega$), and $\Delta\sigma^{\mathrm{exp}}(\vartheta_i)$ is the experimental error. The darker (blue) area in Fig. 3 includes four curves corresponding to $W = W^H$ (of which three curves were obtained without the SO term and one with it), while the gray area includes four curves corresponding to $W = V^F$ (of which two curves were obtained without the SO term and two curves with it). We list in Table I the values of the N parameters χ^2 and the total-reaction cross sections σ_R.

Figure 3 shows the satisfactory overall agreement of both areas of the curves with the experimental data. However, we note the better agreement in the case where $W = W^H$ [darker (blue) area] and the values of χ^2 are between 1.40 and 1.47, while in the case $W = V^F$ they are between 5.00 and 5.80. The situation is similar also for the other energies. So, in our further calculations we use only ImOP $W = W^H$. Second, we note that the values of σ_R are quite different in both cases ($\sigma_R \approx 455$–462 mb for $W = W^H$ and $\sigma_R \approx 260$–390 mb for $W = V^F$). Third, one can see in Table I and from the comparison with the data in Fig. 3 that the role of the SO term is weak. Its effects turn out to be to decrease the values of N_R and to increase the values of N_R^{SO} (see the last two rows in Table I).

As is known, the problem of the ambiguity of parameters N arises when the fitting procedure is applied to a limited number of experimental data (see, e.g., the calculations and discussion

TABLE I. Values of the N parameters, χ^2 and σ_R (in mb), in the case of $^{11}\mathrm{Li} + p$ at 62 MeV/nucleon for the results shown in Fig. 3.

W	N_R	N_I	N_R^{SO}	N_I^{SO}	χ^2	σ_R
W^H	0.871	0.953			1.415	456.97
	0.870	0.965			1.435	459.37
	0.873	0.948			1.423	455.98
	0.854	0.974	0.028	0.000	1.468	461.21
V^F	0.953	0.448			5.567	389.72
	0.956	0.398			5.726	361.02
	0.670	0.251	0.338	0.000	5.027	258.65
	0.623	0.266	0.402	0.000	5.538	270.05

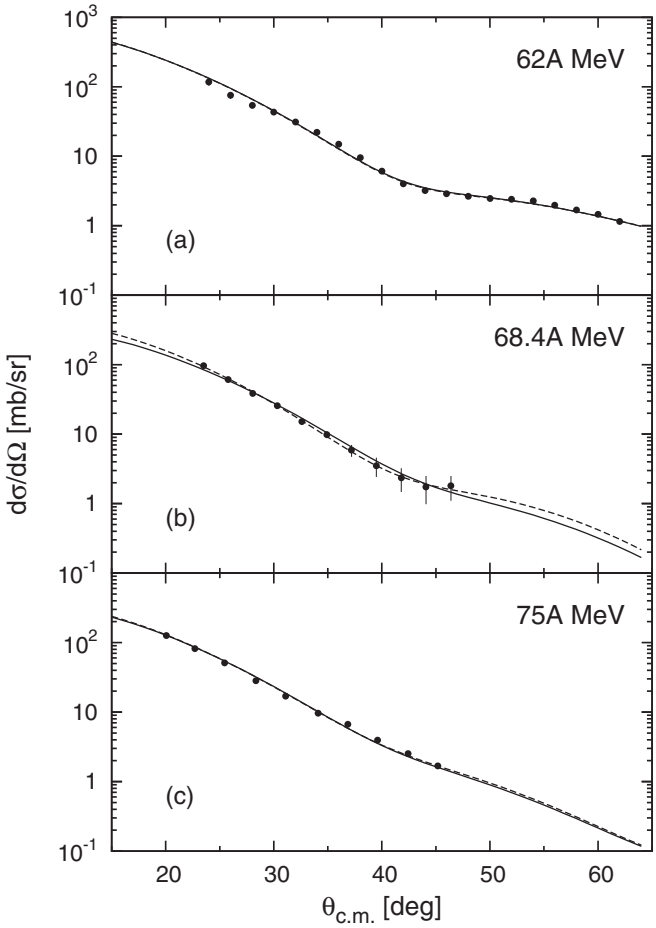

FIG. 4. ^{11}Li + p elastic scattering cross section at $E = 62$, 68.4, and 75 MeV/nucleon. Solid line, without SO term; dashed line, with SO term. Values of N's are listed in Table II. Experimental data are taken from [21] for 62 MeV/nucleon, from [22] for 68.4 MeV/nucleon, and from [23] for 75 MeV/nucleon.

in our previous works [44–46]). Owing to the fact that the fitting procedure belongs to the class of ill-posed problems (see, e.g., Ref. [52]), it becomes necessary to impose some physical constraints on the choice of the set of parameters N. The total cross section of scattering and reaction is one of them, however, the corresponding experimental values are missing at the energy interval considered in the present work.

Another physical criterion that has to be imposed on the choice of N values is the behavior of the volume integrals

$$J_V = \frac{4\pi}{A}\int drr^2[N_R V^F(r)], \tag{12}$$

$$J_W = \frac{4\pi}{A}\int drr^2[N_I W^H(r)] \tag{13}$$

as functions of the energy.

We show in Fig. 4 the results of our calculations of the ^{11}Li + p elastic scattering cross sections for the three energies $E = 62$, 68.4, and 75 MeV/nucleon. For each energy we present two curves, with and without accounting for the SO term. The corresponding values of the N parameters together with those of J_V, J_W, χ^2, and σ_R are listed in Table II. In

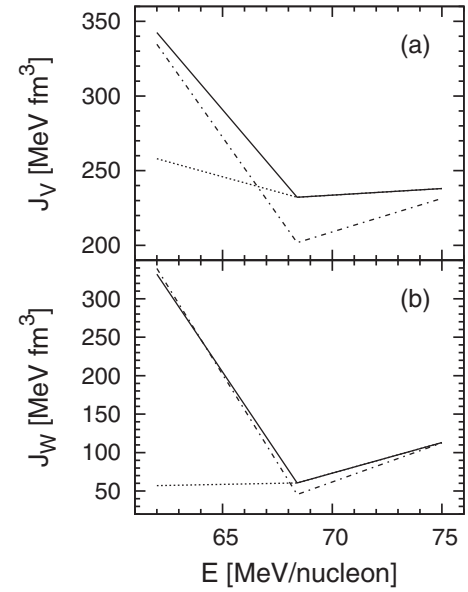

FIG. 5. Values of the volume integrals J_V and J_W [Eqs. (12) and (13)] as functions of the energy per nucleon for ^{11}Li + p elastic scattering. N values are listed in Table II. Solid line, without the SO term of $U_{\rm opt}$ [Eq. (10)]; dash-dotted line, with the SO term of $U_{\rm opt}$. The additional values of J_V and J_W at $E = 62$ MeV/nucleon (connected by a dotted line with the other curves) are obtained in the case where the fitting procedure for the N parameters is limited up to the experimental points for $\theta_{\rm c.m.} \leqslant 46^\circ$ (see text).

Fig. 5 we give the curves for the volume integrals J_V and J_W connecting the results obtained in our calculations with N values. We present them as better ones because, first, the values of χ^2 are around unity and, second, there is a good agreement with the data including those of $\theta_{\rm c.m.}$ up to 60° for 62 MeV/nucleon. One can see that the values of J_V decrease with an increase in the incident energy (with a small exception at 68.4 MeV/nucleon), which is in general agreement with the results in Ref. [53]. This is not the case for J_W, whose value for $E = 62$ MeV/nucleon is larger than for the others. Indeed, it was pointed out in [53] that the general behavior of the volume integral J_V decreases with an increase in the energy in the interval $0 < E < 100$ MeV/nucleon, while J_W increases with an increase in the comparatively low energy and becomes almost constant at a higher energy. However, the same situation occurred in the analysis of the same data at three energies within the semimicroscopic approach in Ref. [37], where the ReOP was calculated using a single-folding procedure with Gaussian, Gaussian-oscillator, and COSMA forms of the single-particle density and the ImOP was taken phenomenologically in a WS form or equal to the form of the folded ReOP. Figure 6(a) shows the curves of J_V corresponding to the values obtained in [37] for the cases of the four densities used. In addition, we show in Fig. 6(b) the values of J_W calculated using the corresponding fitted imaginary part of the OPs taken in a phenomenological WS form. One can see that the J_V shows a reasonable behavior, in agreement with the results in Ref. [53], while the values of J_W are in contradiction to them. Thus, the problem arising in our work appeared also in the semiphenomenological approach in

TABLE II. Values of the N parameters, volume integrals J_V and J_W (in MeV fm^3), χ^2, and total-reaction cross sections σ_R (in mb) for results at three energies E (in MeV/nucleon) considered and shown in Fig. 4.

E	N_R	N_I	N_R^{SO}	N_I^{SO}	J_V	J_W	χ^2	σ_R
62	0.871	0.953			342.474	332.015	1.415	456.97
	0.851	0.974	0.028	0.000	334.610	339.332	1.468	461.21
68.4	0.625	0.186			232.210	60.489	1.328	153.44
	0.543	0.140	0.201	0.000	201.744	45.530	0.316	122.25
75	0.679	0.370			238.048	112.913		232.62
	0.660	0.369	0.045	0.000	231.387	112.607		232.62

Ref. [37], in which a larger number of parameters was used. A possible reason for such behavior of J_W at this energy could be the change in the scattering mechanism with an increase in the angle of scattering when the other channels except the elastic one should be taken into consideration. Such a "strong" channel, with its influence on the elastic one, could be that of the fragmentation of ^{11}Li into clusters.

As the next step, we perform a methodical study of the $^{11}\mathrm{Li} + p$ elastic scattering cross section for $E =$ 62 MeV/nucleon, limiting our fitting procedure for the N parameters up to the experimental points for $\theta_{\mathrm{c.m.}} \leqslant 46^\circ$. The result of this study is presented in Fig. 7. Doing so, we now consider the experimental data for all three energies, 62, 68.4, and 75 MeV/nucleon, being in the same region of angles. The fit to this number of data at 62 MeV/nucleon yields a new set of parameters: $N_R = 0.656$, $N_I = 0.164$ with $\chi^2 = 0.788$, and $\sigma_R = 154.86$ mb. Now we obtain values of the volume integrals (without the SO term of U_{opt}) $J_V = 257.973$ MeV fm^3 and $J_W = 57.136$ MeV fm^3 (shown in Fig. 5), while the values obtained before are $J_V = 342.47$ MeV fm^3 and $J_W = 332.015$ MeV fm^3 (see the first row in Table II). As a result, we get behavior of J_V and J_W in reasonable agreement with the conclusions of Ref. [53]. In our opinion, the procedure described above points out the effect of the data at $\theta_{\mathrm{c.m.}} > 46^\circ$ on the values of χ^2 and on the conclusions regarding the mechanism of the elastic scattering process.

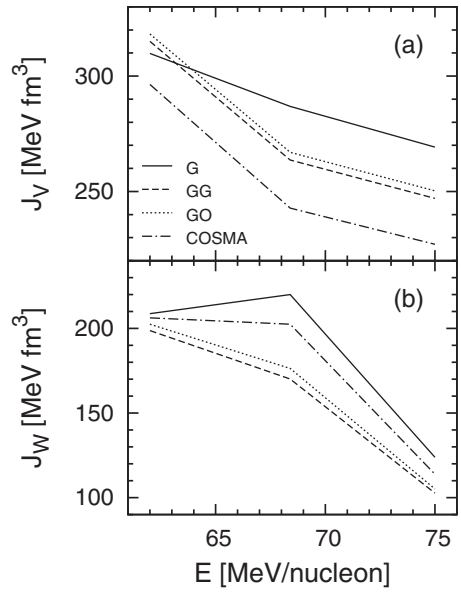

FIG. 6. Energy dependence of the volume integrals. (a) J_V obtained in [37] for folding potentials ReOP (V) calculated using two types of Gaussian (G and GG), Gaussian oscillator (GO), and COSMA densities of ^{11}Li for $^{11}\mathrm{Li} + p$ elastic scattering. (b) J_W calculated using the fitted imaginary WS potentials corresponding to those real parts of OP that give J_V's in (a).

III. BREAKUP PROCESSES WITHIN THE $^9\mathrm{Li} + 2n$ CLUSTER MODEL

A. Two-cluster model and applications

In this section, in addition to the analysis of the $^{11}\mathrm{Li} + p$ elastic scattering cross section in Sec. II, we study other characteristics of the reaction mechanism, such as the ^{11}Li total-reaction cross section, the breakup cross section, and related quantities. This part of the work is based on the procedure for microscopic calculations of OPs presented in Sec. II. We consider a simple two-cluster model that has been used to study ^{6}He elastic scattering and breakup reactions on nuclear targets [54]. Within this model for the ^{11}Li nucleus, first, the density distributions of the ^{9}Li core (c cluster) and $h = 2n$ halo must be given; second, the folding potentials of the interaction of each of the clusters with the incident proton have to be computed; and finally, the sum of these two potentials must be folded with the respective two-cluster density distribution of ^{11}Li, which means that the wave function of the relative

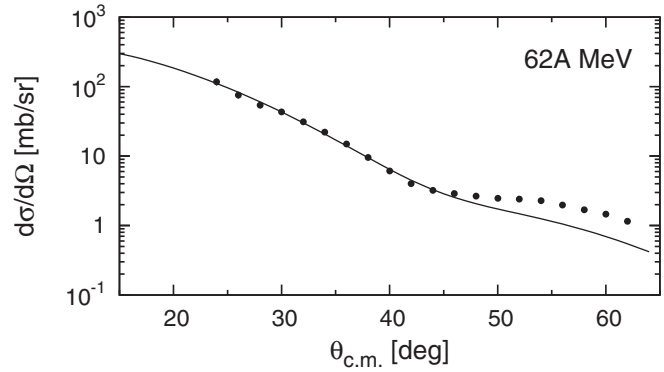

FIG. 7. $^{11}\mathrm{Li} + p$ elastic scattering cross section at $E = 62$ MeV/nucleon when the fitting procedure for the N parameters is limited only up to the experimental points for $\theta_{\mathrm{c.m.}} \leqslant 46^\circ$. Obtained values of N_R, N_I, J_V, J_W, χ^2, and σ_R are given in the text.

motion of two clusters must be known. We calculate the latter as a solution of the Schrödinger wave equation by using the WS potential and given the $0s$ or $1s$ state for particles with a reduced mass of both clusters. WS parameters are obtained by fitting the energy of a given state to the empirical separation energy value of the h cluster $\varepsilon = 0.247$ MeV and the rms radius of the cluster function. For the latter we choose the value of 4.93 fm, which is somehow "in between" the values obtained within the three-body COSMA [55] and deduced from shell-model calculations [56,57]. This two-cluster model takes an interspace between the two classes of approaches. In one of them each of the clusters has its own phenomenological density, which is often used to fit the elastic scattering data. The second class includes microscopic three-body models using, to a different extent, the shell-model picture. Among them we would like to note COSMA (see, for example, Refs. [58] and [59]), which has already successfully described a great number of experimental data applying the Glauber scattering theory. Justifying our simpler two-cluster model, we hope, however, to keep the basic physical consideration avoiding some simplifications like folding without exchange effects, use of Gaussian-type functions for densities of clusters and bound-state wave functions of relative motion, and use of the phenomenological ImOP. We always take into account the contribution of the exchange effects, and the wave function of the relative motion of two clusters is calculated for the fitted finite-range potential that has an exponential behavior. The bound-state two-cluster system requires a particular consideration. In the earlier work estimations were made using the wave function of the $0s$ state ($n = 0$) of the $(c + h)$ system, which does not have nodes inside the potential (except at $r = 0$). However, it has been shown in Refs. [55] and [57] that owing to the violation of the Pauli principle (Pauli-blocking effect in the ^{11}Li ground state), the $1s$ and $0p$ states make the main contribution to the wave function of the two-cluster system, with almost equal probabilities, thus oscillating once inside the potential. Nevertheless, we consider both $0s$ and $1s$ densities $\rho_0^{(0)}$ and $\rho_0^{(1)}$ in further calculations and comparisons of the results.

In the present study, the interaction between the clusters is taken to be a WS potential with the adjusted geometrical parameters $R = 1.0$ fm, $a = 0.25$ fm, and depth $V_0 = 32.55$ MeV for the $0s$ state and $R = 6.25$ fm, $a = 0.25$ fm, and $V_0 = 11.55$ MeV for the $1s$ state.

The s-state ($l = 0$) wave function of the relative motion of two clusters is

$$\phi_{00}^{(n)}(\mathbf{s}) = \phi_0^{(n)}(s)\frac{1}{\sqrt{4\pi}}, \quad n = 0, 1, \tag{14}$$

and thus, the respective density distribution is defined as the probability of clusters being at a mutual distance s:

$$\rho_0^{(n)}(\mathbf{s}) = \left|\phi_{00}^{(n)}(\mathbf{s})\right|^2 = \frac{1}{4\pi}\left|\phi_0^{(n)}(s)\right|^2. \tag{15}$$

In the framework of the $^9\mathrm{Li} + 2n$ model of ^{11}Li one can estimate the $^{11}\mathrm{Li} + p$ OP as a sum of the two OPs of interactions of the c and h clusters with protons folded with the density $\rho_0^{(n)}(s)$ ($n = 0, 1$):

$$\begin{aligned} U^{(b,n)}(r) &= V^{(b,n)} + iW^{(b,n)} \\ &= \int d\mathbf{s}\rho_0^{(n)}(s)\big[U_c^{(n)}(\mathbf{r} + (2/11)\mathbf{s}) \\ &\quad + U_h^{(n)}(\mathbf{r} - (9/11)\mathbf{s})\big] \\ &= 2\pi\int_0^\infty \rho_0^{(n)}(s)s^2 ds \\ &\quad \times \int_{-1}^{1} dx\big[U_c^{(n)}(\sqrt{r^2 + (2s/11)^2 + r(4/11)sx}) \\ &\quad + U_h^{(n)}(\sqrt{r^2 + (9s/11)^2 - r(18/11)sx})\big]. \end{aligned} \tag{16}$$

In Eq. (16), $\mathbf{r} - (9/11)\mathbf{s} \equiv \mathbf{r}_h$ and $\mathbf{r} + (2/11)\mathbf{s} \equiv \mathbf{r}_c$ define the corresponding distances between the centers of each of the clusters and the arbitrary position of the nucleon in the ^{11}Li nucleus, and $\mathbf{s} = \mathbf{s}_1 + \mathbf{s}_2 = (9/11)\mathbf{s} + (2/11)\mathbf{s}$ determines the relative distance between the centers of the two clusters, s_1 and s_2 being the distances between the centers of ^{11}Li and each of the clusters, respectively. The potential $U_c^{(n)}$ in Eq. (16) is calculated within the microscopic hybrid model of the OP described in Secs. III A and II B. For the OP of the h-p interaction we use the sum of two v_{np} potentials as

$$U_h^{(n)} = 2v_{np} = 2v(r)(1 + i\gamma). \tag{17}$$

Such an n-p complex potential was used in the four-body model [25] in calculations of $^{11}\mathrm{Li} + p$ elastic scattering and it was shown that the cross sections are rather insensitive to a precise form of the n-p potential taken in the form [60] (in MeV)

$$v(r) = 120e^{-1.487r^2} - 53.4e^{-0.639r^2} - 27.55e^{-0.465r^2}, \tag{18}$$

with $\gamma = 0.4$.

We also intend to adopt the two-cluster model to calculate breakup reactions of ^{11}Li in collisions with the proton target. To this end the HEA method, which was developed in Refs. [15] and [16] and applied in [54] to the ^{6}He+^{12}C reaction, is used in the present study. For simplicity, the superscript index ($n = 0, 1$) which corresponds to the number of nodes of the relative-motion s-wave function of the two clusters is omitted. To show briefly the eikonal formalism, we start with the probability that after the collision with a proton ($z \to \infty$), cluster h or c with impact parameter b remains in the elastic channel:

$$|S_i(b)|^2 = \exp\left[-\frac{2}{\hbar v}\int_{-\infty}^{\infty} dz W_i(\sqrt{b^2 + z^2})\right], \quad i = c, h, \tag{19}$$

where W is the imaginary part of the microscopic OP, (16). Consequently, the probability of the cluster's being removed from the elastic channel is $(1 - |S|^2)$. Thus, the common probability of both the h and the c clusters leaving the elastic channel of the $^{11}\mathrm{Li} + p$ scattering is $(1 - |S_h|^2)(1 - |S_c|^2)$. After averaging the latter by $\rho_0(s)$ (which characterizes the probability of h and c being at a relative distance s), the total absorbtion cross section is obtained:

$$\sigma_{\mathrm{abs}}^{\mathrm{tot}} = 2\pi\int_0^\infty b_h db_h[1 - |S_h(b_h)|^2][1 - I_c(b_h)], \tag{20}$$

where

$$I_c(b_h) = \int d\mathbf{s}\rho_0(s)|S_c(b_c)|^2. \tag{21}$$

In Eq. (21)

$$b_c = \sqrt{s^2\sin^2\theta + b_h^2 + 2sb_h\sin\theta\cos(\varphi-\varphi_h)} \tag{22}$$

and it comes from the relation $\mathbf{b}_c = \mathbf{b}_h + \mathbf{b}$, with $b = s\sin\theta$ being the projection of $\mathbf{s}$ on the plane normal to the z axis along the straight-line trajectory of the incident nucleus.

In the case of a stripping reaction upon the movement of the h cluster from ^{11}Li to the proton target, one should use the probability of h leaving the elastic channel $[1-|S_h(b_h)|^2]$, and of c continuing its elastic scattering with probability $|S_c(b_c)|^2$. Then the probability of the whole process is $|S_c(b_c)|^2[1-|S_h(b_h)|^2]$, and to get the total stripping cross section one has to average over $\rho_0(s)$ [see Eqs. (20) and (21)]. Similarly, the ^{9}Li transfer can be constructed, and the net contribution of both removal reactions yields the total breakup cross section:

$$\sigma_{\rm bu}^{\rm tot} = 2\pi\int_0^\infty b_h db_h\{|S_h(b_h)|^2 + [1-2|S_h(b_h)|^2]I_c(b_h)\}. \tag{23}$$

The sum of both the absorption [Eqs. (20) and (21)] and the breakup [Eq. (23)] cross sections gives the total-reaction cross section:

$$\sigma_R^{\rm tot} = 2\pi\int_0^\infty b_h db_h[1-|S_h(b_h)|^2 I_c(b_h)]. \tag{24}$$

B. Momentum distributions of fragments

As is known (see, e.g., [15]), the differential and total cross sections (for elastic scattering, as well as for diffractive breakup and absorption) all require calculations of the probability functions of the $\mathbf{k}$-momentum distribution of a cluster in the two-cluster system $d^3P(\mathbf{b},\mathbf{k})/d\mathbf{k}$, which depend on the impact parameter $\mathbf{b}$. The general expression for the probability functions can be written as [15]

$$\frac{d^3P_\Omega(\mathbf{b},\mathbf{k})}{d\mathbf{k}} = \frac{1}{(2\pi)^3}\left|\int d\mathbf{s}\phi_{\mathbf{k}}^*(\mathbf{s})\Omega(\mathbf{b},\mathbf{r}_\perp)\phi_{00}^{(n)}(\mathbf{s})\right|^2, \tag{25}$$

where $\Omega(\mathbf{b},\mathbf{r}_\perp)$ is expressed by means of the two profile functions S_c and S_h [Eq. (19)] of the core and the dineutron clusters, respectively. In Eq. (25), $\phi_{\mathbf{k}}(\mathbf{s})$ is the continuum wave function and $\mathbf{k}$ is the relative momentum of both clusters in their center-of-mass frame. The vector $\mathbf{r}_\perp$ is the projection of the relative coordinate $\mathbf{s}$ between the centers of the two clusters on the plane normal to the z axis mentioned above. The ground-state wave function of the relative motion of the two clusters ϕ_{00} is given for the s state by Eq. (14). For calculations of, e.g., the diffractive cross sections, the continuum wave function $\phi_{\mathbf{k}}$ is expanded in the partial-wave representation. If in this case the distortion in the final channel is neglected, the wave function $\phi_{\mathbf{k}}(\mathbf{s})$ is replaced by a plane wave. Then, following Ref. [15] for the s state ($l=0$) the expression for $d^2P_\Omega(\mathbf{b},\mathbf{k})/dk_Ldk_\perp$ will take the form

$$\frac{d^2P_\Omega(\mathbf{b},\mathbf{k})}{dk_Ldk_\perp} = \frac{k_\perp}{16\pi^3k^2}\left|\int ds\int d(\cos\theta_s)\,g(s)\sin(ks)\times\int d\varphi_s\Omega(\mathbf{b},\mathbf{r}_\perp)\right|^2, \tag{26}$$

with

$$\Omega(\mathbf{b},\mathbf{r}_\perp) = S_c(\mathbf{b}_c)S_h(\mathbf{b}_h). \tag{27}$$

In Eq. (26), $g(s) = r\phi_0^{(n)}(s) = r\sqrt{4\pi\rho_0^{(n)}(s)}$, where $\phi_0^{(n)}$ and $\rho_0^{(n)}$ are given in Eqs. (14) and (15). Hence, the diffraction breakup cross section has the form

$$\left(\frac{d\sigma}{dk_L}\right)_{\rm diff} = \int_0^\infty b_h db_h\int_0^{2\pi}d\varphi_h\int_0^\infty dk_\perp\frac{d^2P_\Omega(\mathbf{k},\mathbf{b})}{dk_Ldk_\perp}, \tag{28}$$

with $d^2P_\Omega(\mathbf{b},\mathbf{k})/dk_Ldk_\perp$ from Eq. (26). The integrations over b_h and φ_h in Eq. (28) mean integration over the impact parameter $\mathbf{b}_h$ of the cluster h with respect to the target.

In the case of the stripping reaction when the h cluster leaves the elastic channel it can be shown (following [15]) that the cross section takes the form

$$\left(\frac{d\sigma}{dk_L}\right)_{\rm str} = \frac{1}{2\pi^2}\int_0^\infty b_h db_h d\varphi_h[1-|S_h(b_h)|^2]\times\int\rho d\rho d\varphi_\rho|S_c(b_c)|^2\times\left[\int_0^\infty dz\cos(k_Lz)\phi_0(\sqrt{\rho^2+z^2})\right]^2. \tag{29}$$

Equation (29) is obtained when the incident nucleus has spin equal to 0 and for the s state of the relative motion of both clusters in the nucleus expressed by Eq. (14) with $\mathbf{s} = \mathbf{r}_c - \mathbf{r}_h$, $\rho = \mathbf{b}_c - \mathbf{b}_h$, $\mathbf{s} = \rho + \mathbf{z}$, and b_c from Eq. (22).

C. Results of calculations for breakup processes

To estimate the ^{11}Li breakup on a proton target, we use the two-cluster model described in Sec. III A. As presented there, we intend to study some observables when the ^{11}Li nucleus with an $h = 2n$-cluster separation energy of 0.247 MeV is considered as a system in the $l=0$ state with principal quantum number $n=0$ or $n=1$. The respective WS potentials $V(s)$ and probabilities $\rho_0^{(n)}(s)$ [Eq. (15)] for the distance s between the clusters in ^{11}Li are shown for both $n=0$ and $n=1$ in Figs. 8(a) and 8(b), respectively. Figure 8(a) shows that the WS potential for $n=0$ is about 2.8 times deeper than that for the case of $n=1$, although the shapes of both potentials are similar. We note also that the half-radius of the $n=1$ potential is equal to 6.25 fm and it is much larger than the 1.01 fm of the $n=0$ potential. Figure 8(b) shows that the two densities differ. Particularly, a steep drop of $n=1$ density is observed at $s\approx 3.8$ fm. Moreover, bearing in mind the results of fitting procedures in phenomenological potentials (e.g., in Ref. [20]) giving an rms radius of about $5\div 6$ fm for the constituent h-cluster density $\rho_h(r)$, we may conclude that

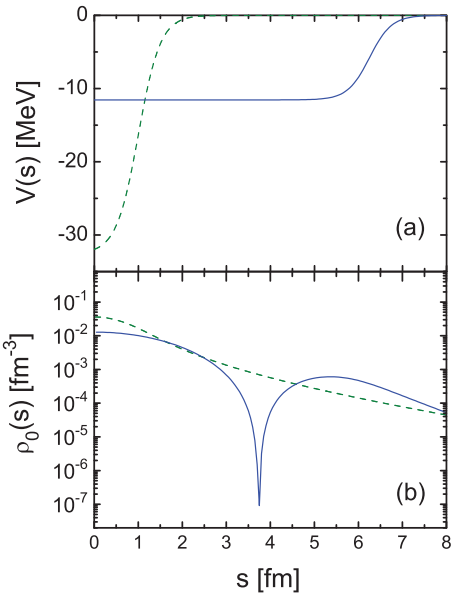

FIG. 8. (Color online) WS potential $V(s)$ of the interaction between the c and the h clusters (a) and the two-cluster density distribution $\rho_0(s)$ normalized to unity (b) for the cases of $n = 0$ [dashed (green) line] and $n = 1$ [solid (blue) line].

in our consideration the $n = 1$ cluster state of ^{11}Li becomes preferable. On the other hand, the existence of long tails of $\rho_0^{(n=0,1)}(s)$ for both states provokes interest in testing their effects in the further considerations.

Our next step is to apply the OP $U^{(b,n)}$ [Eq. (16)] constructed in the framework of the two-cluster model of ^{11}Li to calculate the differential cross section of ^{11}Li + p elastic scattering at 62 MeV/nucleon. For the real part $V^{(b,n)}$ of this OP we use a single-folding procedure in which the LSSM density [43] is taken for the ^{9}Li cluster. The imaginary part $W^{(b,n)}$ of the OP is considered, as before, to be either $W = W^H$ or $W = V^F$. The calculated cross sections are shown in Fig. 9 and compared

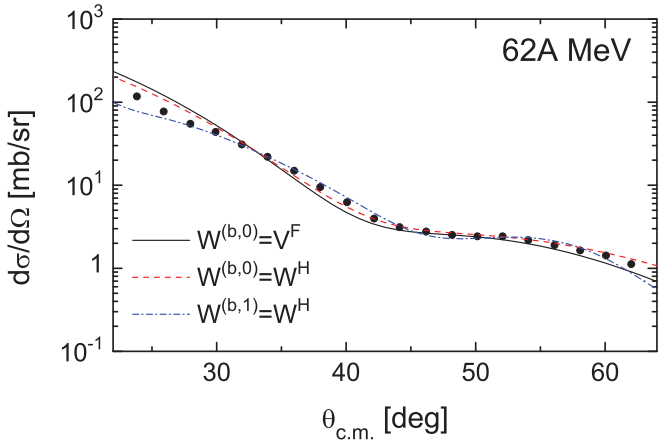

FIG. 9. (Color online) ^{11}Li + p elastic scattering cross section at $E = 62$ MeV/nucleon using $U^{(b,n)}$ [Eq. (16)] for values of the parameters N listed in Table III. Solid black line, $W^{(b,0)} = V^F$; dashed (red) line, $W^{(b,0)} = W^H$; and dash-dotted (blue) line, $W^{(b,1)} = W^H$. Experimental data are taken from Ref. [21].

TABLE III. The N parameters of OPs for ^{11}Li + p scattering at 62 MeV/nucleon and HEA estimations of the total cross sections $\sigma_{\rm abs}^{\rm tot}$ [Eq. (20)], $\sigma_{\rm bu}^{\rm tot}$ [Eq. (23)], and $\sigma_R^{\rm tot}$ [Eq. (24)] (in mb) using the cluster model of ^{11}Li.

$W^{(b,n)}$	N_R	N_I	$\sigma_{\rm abs}^{\rm tot}$	$\sigma_{\rm bu}^{\rm tot}$	$\sigma_R^{\rm tot}$
$W^{(b,0)} = V^F$	1.407	1.195	79.0	431.8	510.8
$W^{(b,0)} = W^H$	1.381	1.306	78.6	405.3	483.9
$W^{(b,1)} = W^H$	4.68	3.99	106.6	581.6	688.2

with the experimental data [21]. For both cases we list in Table III the values of the fitted renormalization coefficient N's and the respective total cross sections for the $n = 0$ and $n = 1$ cases. One can see from Fig. 9 that the angular distributions for both kinds of ImOP are closely displayed and they lead to a fairly good agreement with the experimental data. However, we note that the data are reproduced better again when $W = W^H$ for both the $n = 0$ and the $n = 1$ cases, as pointed out in the discussion of the results presented in Fig. 3 and obtained with the usage of the LSSM density for ^{11}Li.

In Table III the values of the total absorption $\sigma_{\rm abs}^{\rm tot}$, breakup $\sigma_{\rm bu}^{\rm tot}$, and total-reaction $\sigma_R^{\rm tot}$ cross sections are listed. First, we note the significant role that the breakup channel plays in the ^{11}Li + p reaction, where $\sigma_{\rm bu}^{\rm tot}$ contributes more than 80% to $\sigma_R^{\rm tot}$. This is not the case for the ^{6}He+^{12}C process at an energy of 38.3 MeV/nucleon [54], for which the breakup cross section constitutes only about half of the total-reaction cross section. This can be related to the observation that a quite substantial amount of the ^{11}Li + p imaginary potential in the elastic scattering channel is formed owing to a transfer of the incident flux of ^{11}Li to a larger extent into breakup channels. Also, for the case of the $n = 1$ state of the cluster wave function, the fitted strength coefficients N and the respective values of the cross sections are larger than for the $n = 0$ state, but the general conclusions on the preferable role of breakup processes remain the same.

Our next step is to calculate, using Eqs. (28) and (29) as examples, the cross sections of the diffractive and stripping (when $h = 2n$ cluster leaves the elastic channel) ^{11}Li + p reactions at $E = 62$ MeV/nucleon, respectively. For this purpose we use in Eqs. (28) and (29) the corresponding functions $S_i(b_i)$, $i = c, h$ [see Eq. (19)]. They are given in Fig. 10 for the s state with $n = 0$ and $n = 1$. In Figs. 11 and 12 we show the results for the diffraction breakup and stripping ^{11}Li + p scattering at $E = 62$ MeV/nucleon, respectively. These results give predictions because of missing experimental data for such processes accompanying the ^{11}Li + p scattering at $E \leqslant 100$ MeV/nucleon. For the diffractive scattering we obtain values of the widths 98 MeV/c (for $n = 0$) and 85 MeV/c (for $n = 1$), and for the stripping reaction 79 MeV/c (for $n = 0$) and 72 MeV/c (for $n = 1$), respectively, thus favoring the configuration in which the two valence neutrons occupy the $1s$ state in ^{11}Li. It is noteworthy that the widths calculated in our work for the ^{11}Li breakup on the proton target are larger than those obtained in experiments (around 50 MeV/c) for the reactions of ^{11}Li on the nuclear targets ^{9}Be, ^{93}Nb, and ^{181}Ta at an energy of 66 MeV/nucleon [11] and on a wide range of targets (^{9}Be to ^{238}U) [12]. It is noted

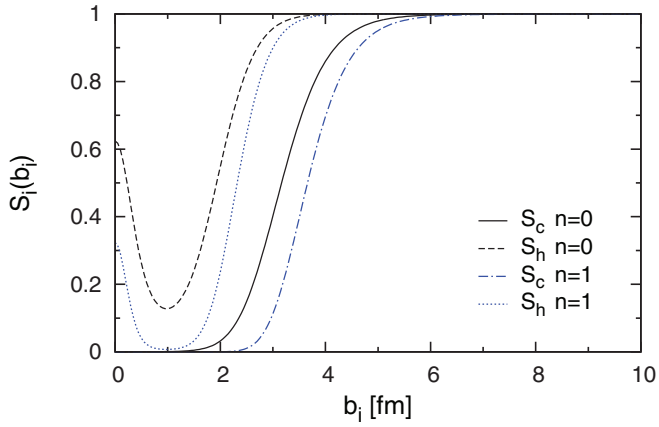

FIG. 10. (Color online) Functions $S_i(b_i)$, $i = c, h$ [see Eq. (19)], for the s state of the relative motion of clusters with $n = 0$ and $n = 1$.

in [11] and [12] that the width almost does not depend on the target's mass number, and thus, it characterizes basically the momentum distribution of two clusters. Our width for the stripping of the $2n$ cluster is similar to the cases of $2n$ stripping from other nuclei (but not from ^{11}Li). It turns out that the account for $2n$ binding in ^{11}Li is not enough to obtain the observed widths in the scattering of ^{11}Li on nuclei, as well as on proton targets. We would like to mention also that we had a methodical task to calculate the widths using different wave functions ($n = 0, 1$) of the relative motion of the clusters. The results show similar values of the widths in both cases. Probably, it is difficult to solve the problem within our simplified two-cluster model, and thus, it must be considered in a more complicated three-body model. Also, obviously, experiments on stripping and diffraction reactions of ^{11}Li on proton targets are highly desirable. This concerns measurements of the neutrons in the decay as well.

D. Single-particle density of ^{11}Li in the two-cluster model

In this subsection we consider in more detail the single-particle density distribution of ^{11}Li that can be calculated and

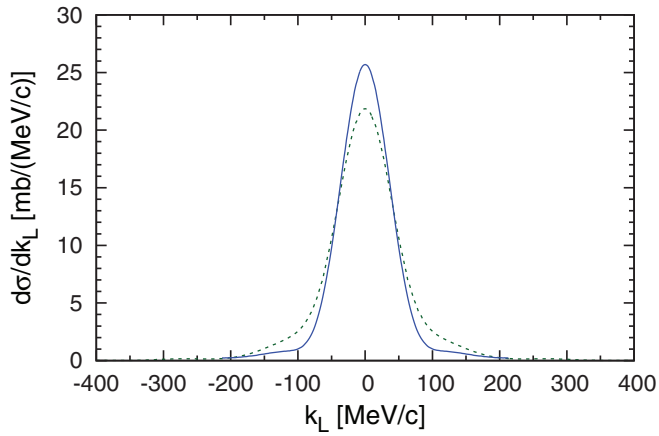

FIG. 11. (Color online) Cross section of diffraction breakup in ^{11}Li + p scattering at $E = 62$ MeV/nucleon for the cases of $n = 0$ [dashed (green) line] and $n = 1$ [solid (blue) line].

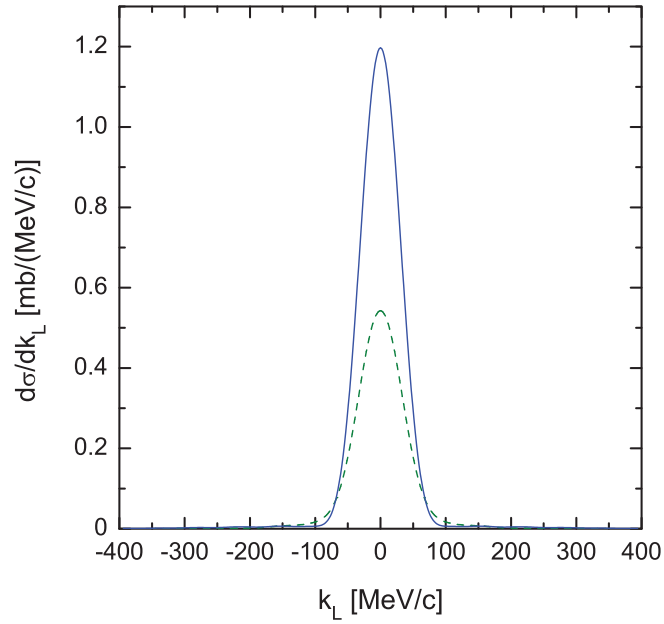

FIG. 12. (Color online) The same as Fig. 11, but for the stripping reaction.

applied, instead of the phenomenological one, in the analyses and interpretation of ^{11}Li + p experimental data. For this purpose, we adopt our cluster model, consisting of a ^{9}Li core and halo $h = 2n$. If one sets $\rho_h(\mathbf{r}_1)$ for the h cluster and $\rho_c(\mathbf{r}_2)$ for the ^{9}Li nucleus, the single-particle density distribution of ^{11}Li can be derived in analogy to Eq. (16) in the following form:

$$\begin{aligned}\rho(r) &= \int d\phi \sin\theta d\theta \int dss^2 \left[\rho_h(\mathbf{r}_h) + \rho_c(\mathbf{r}_c)\right] \rho_0^{(n)}(\mathbf{s}) \\ &= 2\pi \int_{-1}^{1} dx \int_0^{\infty} dss^2 [\rho_h(\sqrt{r^2 - 2(9/11)rsx + (9/11)^2 s^2}) \\ &\quad + \rho_c(\sqrt{r^2 + 2(2/11)rsx + (2/11)^2 s^2})]\rho_0^{(n)}(\mathbf{s}). \qquad (30)\end{aligned}$$

Expression (30) indicates that the density of ^{11}Li can be calculated using the sum of the corresponding densities of both clusters and folding it with the square of the relative-motion wave function of the two clusters $|\phi_{00}(\mathbf{s})|^2$.

As a comment on our approach we would like to mention the difference between the method used to calculate the folding ^{11}Li + p OP [Eq. (16)] and that used to estimate the single-particle density of ^{11}Li [Eq. (30)]. In fact, in the former, the U_h OP was not calculated as a folding integral, but expressed through the v_{np} potentials, and therefore there we did not include the density of the $h = 2n$ cluster. Instead, in Eq. (30) we consider the h-cluster density, together with the density of the ^{9}Li core, both being folded by the wave function of the relative motion of the two clusters.

Further, in the calculations we use the LSSM density for the ^{9}Li cluster with rms radius $R_c = 2.31$ fm [43] and for the h halo we probe two densities: one is described by the Gaussian

TABLE IV. Values of the parameters of the symmetrized Fermi and Gaussian density distributions, h- and c-cluster rms radii R_h and R_c, and deduced matter rms radii R_m (in fm) within the $^9\mathrm{Li}+2n$ model of ^{11}Li.

Parametrization	R	a	R_h	R_c	R_m
SF1	2.234	0.27	2	2.31[a]	2.77 ($n=0$)
					2.93 ($n=1$)
G			2	2.31[a]	2.77 ($n=0$)
					2.93 ($n=1$)
SF2	4.573	0.5	4	2.31[a]	3.32 ($n=1$)
0.2GG + 0.8GO [20]			5.98	2.52	3.42

[a]From the LSSM for ^{9}Li.

function (G density) (e.g., [61])

$$\rho^G(r)=\left(\frac{3}{2\pi R_h^2}\right)^{3/2}\exp\left(-\frac{3r^2}{2R_h^2}\right), \tag{31}$$

and the other is the symmetrized Fermi distribution (SF density) (e.g., [62])

$$\rho^{\mathrm{SF}}(r)=\rho_0\frac{\sinh(R/a)}{\cosh(R/a)+\cosh(r/a)}, \tag{32}$$

where

$$\rho_0=\frac{3}{4\pi R^3}\left[1+\left(\frac{\pi a}{R}\right)^2\right]^{-1}, \tag{33}$$

and the corresponding rms radius is

$$\langle r^2\rangle=R_h^2=\frac{3}{5}R^2\left[1+\frac{7}{3}\left(\frac{\pi a}{R}\right)^2\right]. \tag{34}$$

The two densities [Eqs. (31) and (32)] are normalized to unity, and substituting them in Eq. (30) they have to be multiplied by a factor of 2. As for the G density it has only one parameter that governs its behavior: the rms radius of the halo R_h. First, we take $R_h=2$ fm, which is almost twice the nucleon radius. In principle, such a choice of R_h is justified, as the cluster inside the nucleus is "smeared," and moreover, the folding procedure itself [in which the relative motion function $\phi_{00}(\mathbf{s})$ takes place with rms radius 4.93 fm; see also Sec. III A] ensures that the h cluster is in the periphery. Concerning the SF density, we perform calculations with a set of parameters R and a, selected so as to obey rms $R_h=2$ fm (see the set SF1 in Table IV). For the choice of them the condition $R>\pi a$ must be satisfied, and for more convenience Eq. (34) can be rewritten in the following way:

$$R^2=\tfrac{5}{3}R_h^2-\tfrac{7}{3}(\pi a)^2. \tag{35}$$

The calculated single-particle density distributions of ^{11}Li are presented in Fig. 13 together with the LSSM density. Results are shown for both the $n=0$ and the $n=1$ cases. As shown, the usage of two kinds of h density, SF1 and G, yields very similar ^{11}Li densities, shown as the pair of dotted and dashed curves for $n=0$ and, also, as the solid and dot-dashed curves for $n=1$, correspondingly, in the whole region of r up to 10 fm. In addition, all four curves are close at $r<4$ fm. However, the difference between the $n=0$ and the $n=1$ pairs is seen in the interval $5<r<7$ fm, where the $n=1$ curves

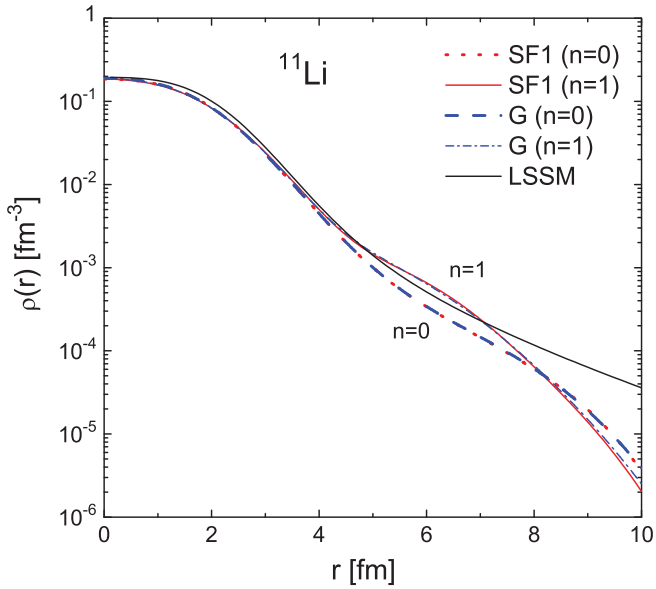

FIG. 13. (Color online) Single-particle density distribution of ^{11}Li (normalized to $A=11$) obtained in the framework of the cluster model [Eq. (30)]. The h-cluster density distributions are taken in two forms: the symmetrized Fermi distribution (SF1) and the Gaussian function (G) with $R_h=2$ fm. Results are presented for the cases of $n=0$ and $n=1$, respectively. The LSSM density is also given.

exhibit a "bump," while the $n=0$ curves go down compared to the case of the LSSM density of ^{11}Li. Moreover, we note that the ^{11}Li rms radius of 2.93 fm for $n=1$ curves is very close to the LSSM value of 2.94 fm. The tail of the LSSM density is higher at $r>8$ fm than those of the cluster curves with $R_h=2$ fm, but as pointed out in Ref. [20] the calculated differential cross sections of $^{11}\mathrm{Li}+p$ scattering are not sensitive to a possible long density tail at the nuclear far periphery.

The very pronounced halo nature of the ^{11}Li nucleus is mainly supported by its large matter radius demonstrated by Tanihata *et al.* in Ref. [1]. Recently, a successful attempt to get a "realistic" density of this nucleus was realized in Ref. [20]. In the latter the experimental data at about 700 MeV/nucleon were described using the phenomenological constituent cluster model of the ^{11}Li density composed of two terms 0.2GG + 0.8GO with the Gaussian GG and the harmonic oscillator GO functions together. The fitting procedure led to the total rms matter radius $R_m=3.42$ fm of the whole density, where the fitted values $R_c=2.52$ fm and $R_h=5.98$ fm of its separate terms were interpreted as the core and h-halo radii, respectively. These radii satisfy the relation

$$R_m^2=\frac{A_cR_c^2+A_hR_h^2}{A},\quad A=A_c+A_h \tag{36}$$

(A_c, A_h, and A being the number of nucleons in the core, the $2n$-cluster, and the nucleus, respectively) that is valid for the constituent model. However, instead, we may argue that the ^{9}Li and h systems can be considered the true clusters only when, in a cluster model, they are folded [see Eq. (30)] with the probability density of their relative motion. In Fig. 14

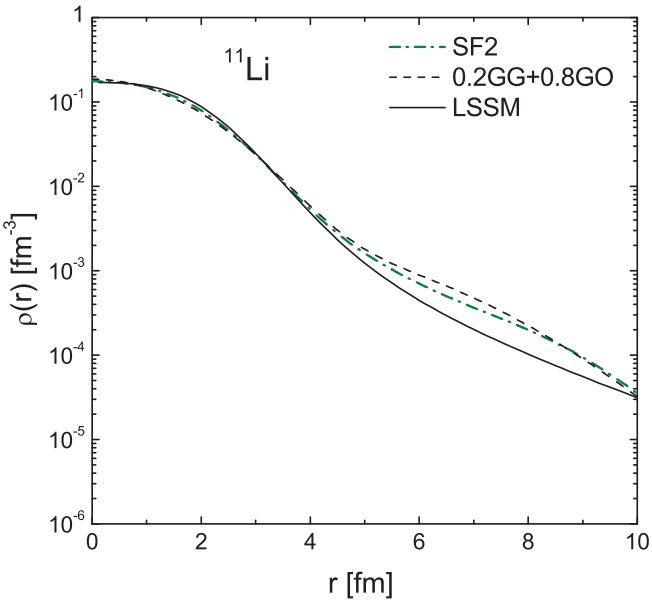

FIG. 14. (Color online) Single-particle density distribution of ^{11}Li (normalized to $A = 11$) obtained in the framework of the cluster model [Eq. (30)] with a symmetrized Fermi (SF2) distribution for the h-cluster density with $R_h = 4$ fm [dash-dotted (green) line]. The dashed black line represents the best density parametrization that describes the $^{11}\mathrm{Li} + p$ elastic scattering data [20]; the solid black line, the LSSM density.

our result is shown as the SF2 curve when the value of $R_h = 4$ fm is taken to be twice as large as the $R_h = 2$ fm in the SF1 case. Also in the same figure we present the phenomenological 0.2GG + 0.8GO density from Ref. [20]. Our SF2 parametrization leads to a value for the matter rms radius $R_m = 3.32$ fm that is close to the $R_m = 3.42$ fm for the phenomenological constituent model mentioned above. Thus, our folding method to calculate the single-particle density distribution [Eq. (30)] which takes into account the relative motion of the clusters makes it possible to get realistic densities within cluster models without the use of phenomenology. It is seen from our analysis with SF2 parametrization that the h cluster is really "smeared" in the ^{11}Li nucleus ($R_h = 4$ fm) and that the averaging on a relative motion of both clusters (which strongly depends on the h-cluster separation energy) plays an important role. This fact is confirmed also in Ref. [20], where the deduced halo radius $R_h = 5.98$ fm is larger than the core radius $R_c = 2.52$ fm by a factor of more than 2. However, the ambiguity remains in the choice of the "best" density distribution of ^{11}Li because only the $^{11}\mathrm{Li} + p$ elastic scattering data are not sufficient.

IV. CONCLUSIONS

The results of the present work can be summarized as follows.

(i) In Sec. II the microscopic OPs and cross sections of $^{11}\mathrm{Li} + p$ elastic scattering have been calculated at the energies of 62, 68.4, and 75 MeV/nucleon and were compared with the available experimental data. The direct (V^D) and exchange (V^{EX}) parts of the real OP (V^F) are calculated using the folding procedure with the density-dependent M3Y (CDM3Y6-type) effective interaction based on the Paris NN potential. The imaginary part of the OP (W^H) has been calculated microscopically within the folding model based on the HEA. The LSSM densities [43] of protons and neutrons with exponential asymptotic behavior of ^{11}Li, which is the correct one, are used in the calculations. The spin-orbit contribution to the OP is also included in the calculations. The $^{11}\mathrm{Li} + p$ elastic scattering cross sections and the total-reaction cross sections are calculated using the program DWUCK4 [48].

(ii) We point out that the regularization of our microscopic OPs is achieved by introducing the fitting parameters N_R, N_I, N_R^{SO}, and N_I^{SO} related to the "depths" of the separate parts of the OP. They are, in principle, the only free parameters of our approach, in contrast to other phenomenological ones, and serve as a quantitative test of the latter; i.e., the proximity of N values to unity shows the closeness of the approach to reality. However, here the "ill-posed" problem takes place because the fitting procedure is applied to a limited number of experimental data. The problem of the ambiguity of the N parameters has been considered in our previous work [45,46]. In the present work we use a physical constraint on the choice of the values of the N parameters, namely, the known behavior of the volume integrals J_V and J_W as functions of the incident energy for $E \leqslant 100$ MeV/nucleon [53]. We compare the behaviors of the values of J_V and J_W obtained in our work with those in the semiphenomenological approach in Ref. [37], where many more parameters have been used than in our microscopic method. We discuss in more detail the problem arising from the behavior of J_W at $E = 62$ MeV/nucleon and relate it to the quality of the data at larger angles ($\theta_{\mathrm{c.m.}} > 46^\circ$). We note that this problem appeared also in [37]. Finally, we obtained a definite set of the fitted N parameters that give satisfactory agreement of our results with the data on the $^{11}\mathrm{Li} + p$ elastic scattering cross section using the physical criterion of the behavior of the volume integrals as a function of the energy.

(iii) We would like to mention that the values of the total cross sections of scattering and reaction can serve as another physical criterion for the N values. However, the corresponding experimental data for these values are missing at the energy interval considered in our work, so they are highly desirable.

(iv) As in our previous work [45,46], we would like to emphasize that a more successful explanation of the cross-section data could be given by accounting for virtual excitations of inelastic and decay channels of the reaction. For this reason, in Sec. III of the present paper, apart from the usual folding model based on the LSSM, we consider another folding approach, which includes ^{11}Li breakup, suggesting a simple $^{9}\mathrm{Li} + 2n$ cluster model for its structure. Both LSSM and cluster models of ^{11}Li are capable of reproducing fairly well the two-neutron separation energy from ^{11}Li. In Sec. III we use the procedure from Sec. II for microscopic calculations of the necessary OPs in the breakup model for estimations of the elastic scattering cross sections, as well as of the momentum distributions in the processes of proton scattering on clusters and the corresponding S functions in $^{9}\mathrm{Li} + p$ and $h + p$ scattering. The folding

OPs calculated in the two parts of our work behave rather closely if one fits their strengths to the same elastic scattering data as done for $^{11}\mathrm{Li} + p$ at an energy of 62 MeV/nucleon. Thus, the analysis of other types of reaction mechanism, such as ^{11}Li breakup, makes it possible to understand their significant role in the formation of the OP responsible for $^{11}\mathrm{Li} + p$ elastic scattering. It turns out that the breakup channel gives a $\sigma_{\mathrm{bu}}^{\mathrm{tot}}$ that exceeds 80% of σ_R^{tot}, while it is about a half of σ_R^{tot} in the case of ^{6}He+^{12}C (as obtained in Ref. [54]).

(v) In the present work we also give predictions for the longitudinal momentum distributions of ^{9}Li fragments produced in the breakup of ^{11}Li at 62 MeV/nucleon on a proton target. We have calculated the diffraction and stripping (when the cluster $2n$ leaves the elastic channel) cross sections of the reaction of ^{11}Li on a proton target at an energy of 62 MeV/nucleon. We note that our breakup gives the width of the peak as between 70 and 80 MeV/c, while widths of about 50 MeV/c are known from the reactions of ^{11}Li on nuclear targets ^{9}Be, ^{93}Nb, and ^{181}Ta at an energy of 66 MeV/nucleon. In relation to this, here we should mention that at an energy in the range 60–70 MeV/nucleon a distortion owing to the nuclear and Coulomb forces could affect the cross sections. We have in mind also that our simplified two-cluster model could not give the correct answer and that it can be found in a more complicated three-body approach. Hence, this problem remains open and requires further analysis. We emphasize the necessity for experiments on stripping and diffraction reactions of ^{11}Li on proton targets at an energy $E < 100$ MeV/nucleon.

(vi) We present results for the single-particle density distribution of ^{11}Li in the framework of a cluster model. Our calculated density is close to the phenomenological one obtained in Ref. [20] by fitting to the experimental differential cross sections of scattering of ^{11}Li at 700 MeV/nucleon on a proton target. From a physical point of view the cluster model allows more clear interpretation of the experimental data, and together with the phenomenological densities, it can be applied as a pattern density to fit the data. Future measurements of the cross sections for proton elastic scattering and momentum distribution of ^{9}Li fragments in ^{11}Li breakup reactions might provide supplemental information on the internal spatial structure of the ^{11}Li nucleus.

ACKNOWLEDGMENTS

The authors are grateful to Professor N. S. Zelenskaya and Professor S. N. Ershov for helpful discussions. The work was partly supported by the project from the agreement for cooperation between the INRNE-BAS (Sofia) and JINR (Dubna). Four of the authors (D.N.K., A.N.A., M.K.G., and K.S.) are grateful for the support of the Bulgarian Science Fund under Contract No. 02–285, and one of them (D.N.K.), for support under Contract No. DID–02/16–17.12.2009. E.V.Z. and K.V.L. thank the Russian Foundation for Basic Research (Grant Nos. 12-01-00396 and 13-01-00060) for partial support. K.S. acknowledges the support of Project BG-051P0001-3306-003.

[1] I. Tanihata, H. Hamagaki, O. Hashimoto, S. Nagamiya, Y. Shida, N. Yoshikawa, O. Yamakawa, K. Sugimoto, T. Kobayashi, D. E. Greiner, N. Takahashi, and Y. Nojiri, Phys. Lett. B **160**, 380 (1985).

[2] I. Tanihata, H. Hamagaki, O. Hashimoto, Y. Shida, N. Yoshikawa, K. Sugimoto, O. Yamakawa, T. Kobayashi, and N. Takahashi, Phys. Rev. Lett. **55**, 2676 (1985).

[3] I. Tanihata, T. Kobayashi, O. Yamakawa, T. Shimoura, K. Ekuni, K. Sugimoto, N. Takahashi, T. Shimoda, and H. Sato, Phys. Lett. B **206**, 592 (1988).

[4] W. Mittig, J. M. Chouvel, Z. W. Long, L. Bianchi, A. Cunsolo, B. Fernandez, A. Foti, J. Gastebois, A. Gillibert, C. Gregoire, Y. Schutz, and C. Stephan, Phys. Rev. Lett. **59**, 1889 (1987).

[5] P. G. Hansen and B. Jonson, Eur. Lett. **4**, 409 (1987).

[6] A. B. Migdal, Sov. J. Nucl. Phys. **16**, 238 (1973).

[7] T. Kobayashi, O. Yamakawa, K. Omata, K. Sugimoto, T. Shimoda, N. Takahashi, and I. Tanihata, Phys. Rev. Lett. **60**, 2599 (1988).

[8] G. F. Bertsch, B. A. Brown, and H. Sagawa, Phys. Rev. C **39**, 1154 (1989); T. Hoshino, H. Sagawa, and A. Arima, Nucl. Phys. A **506**, 271 (1990); L. Johannsen, A. S. Jensen, and P. G. Hansen, Phys. Lett. B **244**, 357 (1990); A. C. Hayes, *ibid*. **254**, 15 (1991); G. F. Bertsch and H. Esbensen, Ann. Phys. **209**, 327 (1991); Y. Tosaka and Y. Suzuki, Nucl. Phys. A **512**, 46 (1990).

[9] R. Anne *et al*., Phys. Lett. B **250**, 19 (1990).

[10] H. Esbensen, Phys. Rev. C **44**, 440 (1991); **53**, 2007 (1996).

[11] N. A. Orr, N. Anantaraman, Sam M. Austin, C. A. Bertulani, K. Hanold, J. H. Kelley, D. J. Morrissey, B. M. Sherrill, G. A. Souliotis, M. Thoennessen, J. S. Winfield, and J. A. Winger, Phys. Rev. Lett. **69**, 2050 (1992).

[12] N. A. Orr, N. Anantaraman, Sam M. Austin, C. A. Bertulani, K. Hanold, J. H. Kelley, R. A. Kryger, D. J. Morrissey, B. M. Sherrill, G. A. Souliotis, M. Steiner, M. Thoennessen, J. S. Winfield, J. A. Winger, and B. M. Young, Phys. Rev. C **51**, 3116 (1995).

[13] D. Baye and P. Capel, Lect. Notes Phys. **848**, 121 (2012).

[14] F. Barranco, E. Vigezzi, and R. A. Broglia, Z. Phys. A **356**, 45 (1996).

[15] K. Hencken, G. Bertsch, and H. Esbensen, Phys. Rev. C **54**, 3043 (1996).

[16] C. A. Bertulani and P. G. Hansen, Phys. Rev. C **70**, 034609 (2004).

[17] C. A. Bertulani and K. W. McVoy, Phys. Rev. C **46**, 2638 (1992).

[18] S. N. Ershov, B. V. Danilin, J. S. Vaagen, A. A. Korsheninnikov, and I. J. Thompson, Phys. Rev. C **70**, 054608 (2004).

[19] C. A. Bertulani, M. Hussein, and G. Muenzenberg, *Physics of Radioactive Beams* (Nova Science, Hauppage, NY, 2002).

[20] A. V. Dobrovolsky, G. D. Alkhazov, M. N. Andronenko, A. Bauchet, P. Egelhof, S. Fritz, H. Geissel, C. Gross, A. V. Khanzadeev, G. A. Korolev, G. Kraus, A. A. Lobodenko, G. Münzenberg, M. Mutterer, S. R. Neumaier, T. Schäfer, C. Scheidenberger, D. M. Seliverstov, N. A. Timofeev, A. A. Vorobyov, and V. I. Yatsoura, Nucl. Phys. A **766**, 1 (2006).

[21] C.-B. Moon, M. Fujimaki, S. Hirenzaki, N. Inabe, K. Katori, J. C. Kim, Y. K. Kim, T. Kobayashi, T. Kubo, H. Kumagai, S. Shimoura, T. Suzuki, and I. Tanihata, Phys. Lett. B **297**, 39 (1992).

[22] A. A. Korsheninnikov, E. A. Kuzmin, E. Yu. Nikolskii, O. V. Bochkarev, S. Fukuda, S. A. Goncharov, S. Ito, T. Kobayashi, S. Momota, B. G. Novatskii, A. A. Ogloblin, A. Ozawa, V. Pribora, I. Tanihata, and K. Yoshida, Phys. Rev. Lett. **78**, 2317 (1997).
[23] A. A. Korsheninnikov, E. Yu. Nikolskii, T. Kobayashi, A. Ozawa, S. Fukuda, E. A. Kuzmin, S. Momota, B. G. Novatskii, A. A. Ogloblin, V. Pribora, I. Tanihata, and K. Yoshida, Phys. Rev. C **53**, R537 (1996).
[24] M. V. Zhukov, B. V. Danilin, D. V. Fedorov, J. M. Bang, I. J. Thompson, and J. S. Vaagen, Phys. Rep. **231**, 151 (1993).
[25] Y. Suzuki, K. Yabana, and Y. Ogawa, Phys. Rev. C **47**, 1317 (1993).
[26] M. Kohno, Phys. Rev. C **48**, 3122 (1993).
[27] A. K. Chaudhuri, Phys. Rev. C **49**, 1603 (1994).
[28] R. Kanungo and C. Samanta, Nucl. Phys. A **617**, 265 (1997).
[29] Y. J. Kim and M. H. Cha, Int. J. Mod. Phys. E **10**, 91 (2001).
[30] R. Crespo, J. A. Tostevin, and I. J. Thompson, Phys. Rev. C **54**, 1867 (1996).
[31] K. Amos, W. A. Richter, S. Karataglidis, and B. A. Brown, Phys. Rev. Lett. **96**, 032503 (2006); P. K. Deb, B. C. Clark, S. Hama, K. Amos, S. Karataglidis, and E. D. Cooper, Phys. Rev. C **72**, 014608 (2005).
[32] M. Avrigeanu, G. S. Anagnostatos, A. N. Antonov, and J. Giapitzakis, Phys. Rev. C **62**, 017001 (2000); M. Avrigeanu, G. S. Anagnostatos, A. N. Antonov, and V. Avrigeanu, Int. J. Mod. Phys. E **11**, 249 (2002); M. Avrigeanu, A. N. Antonov, H. Lenske, and I. Stetcu, Nucl. Phys. A **693**, 616 (2001).
[33] G. R. Satchler and W. G. Love, Phys. Rep. **55**, 183 (1979); G. R. Satchler, *Direct Nuclear Reactions* (Clarendon Press, Oxford, UK, 1983).
[34] D. T. Khoa and W. von Oertzen, Phys. Lett. B **304**, 8 (1993); **342**, 6 (1995); D. T. Khoa, W. von Oertzen, and H. G. Bohlen, Phys. Rev. C **49**, 1652 (1994); D. T. Khoa, W. von Oertzen, and A. A. Ogloblin, Nucl. Phys. A **602**, 98 (1996); D. T. Khoa and H. S. Than, Phys. Rev. C **71**, 044601 (2005); O. M. Knyaz'kov, Sov. J. Part. Nucl. **17**, 137 (1986).
[35] D. T. Khoa and G. R. Satchler, Nucl. Phys. A **668**, 3 (2000).
[36] D. T. Khoa, G. R. Satchler, and W. von Oertzen, Phys. Rev. C **56**, 954 (1997).
[37] M. Y. M. Hassan, M. Y. H. Farag, E. H. Esmael, and H. M. Maridi, Phys. Rev. C **79**, 014612 (2009).
[38] M. Y. H. Farag, E. H. Esmael, and H. M. Maridi, Eur. Phys. J. A **48**, 154 (2012).
[39] K. V. Lukyanov, E. V. Zemlyanaya, and V. K. Lukyanov, Phys. At. Nucl. **69**, 240 (2006); JINR Preprint P4-2004-115, Dubna, 2004.
[40] P. Shukla, Phys. Rev. C **67**, 054607 (2003).
[41] R. J. Glauber, in *Lectures in Theoretical Physics* (Interscience, New York, 1959), p. 315.
[42] A. G. Sitenko, Ukr. Fiz. J. **4**, 152 (1959).
[43] S. Karataglidis, P. G. Hansen, B. A. Brown, K. Amos, and P. J. Dortmans, Phys. Rev. Lett. **79**, 1447 (1997); S. Karataglidis, P. J. Dortmans, K. Amos, and C. Bennhold, Phys. Rev. C **61**, 024319 (2000).
[44] K. V. Lukyanov, V. K. Lukyanov, E. V. Zemlyanaya, A. N. Antonov, and M. K. Gaidarov, Eur. Phys. J. A **33**, 389 (2007).
[45] V. K. Lukyanov, E. V. Zemlyanaya, K. V. Lukyanov, D. N. Kadrev, A. N. Antonov, M. K. Gaidarov, and S. E. Massen, Phys. Rev. C **80**, 024609 (2009).
[46] V. K. Lukyanov, D. N. Kadrev, E. V. Zemlyanaya, A. N. Antonov, K. V. Lukyanov, and M. K. Gaidarov, Phys. Rev. C **82**, 024604 (2010).
[47] V. K. Lukyanov, D. N. Kadrev, E. V. Zemlyanaya, A. N. Antonov, K. V. Lukyanov, M. K. Gaidarov, and K. Spasova, Phys. At. Nucl. **75**, 1407 (2012).
[48] P. D. Kunz and E. Rost, in *Computational Nuclear Physics*, edited by K. Langanke *et al*., Vol. 2 (Springer-Verlag, New York, 1993), p. 88.
[49] P. Shukla, arXiv:nucl-th/0112039.
[50] S. K. Charagi and S. K. Gupta, Phys. Rev. C **41**, 1610 (1990); **46**, 1982 (1992).
[51] C. Xiangzhow, F. Jun, S. Wenqing, M. Yugang, W. Jiansong, and Y. Wei, Phys. Rev. C **58**, 572 (1998).
[52] A. N. Tikhonov and V. Y. Arsenin, *Solutions of Ill-Posed Problems* (V. H. Winston and Sons, Wiley, New York, 1977).
[53] E. A. Romanovsky *et al*., Bull. Russ. Acad. Sci.: Phys. **62**, 150 (1998).
[54] V. K. Lukyanov, E. V. Zemlyanaya, and K. V. Lukyanov, Int. J. Mod. Phys. E **20**, 2039 (2011).
[55] I. J. Thompson and M. V. Zhukov, Phys. Rev. C **49**, 1904 (1994).
[56] L. I. Galanina and N. S. Zelenskaya, Bull. Russ. Acad. Sci.: Phys. **77**, 383 (2013); Phys. At. Nucl. **76**, 12 (2013).
[57] T. Myo, K. Kato, H. Toki, and K. Ikeda, Phys. Rev. C **76**, 024305 (2007).
[58] J. A. Tostevin, R. C. Johnson, and J. S. Al-Khalili, Nucl. Phys. A **630**, 340c (1998).
[59] S. N. Ershov, L. V. Grigorenko, J. S. Vaagen, and M. V. Zhukov, J. Phys. G **37**, 064026 (2010).
[60] D. R. Thompson, M. LeMere, and Y. C. Tang, Nucl. Phys. A **286**, 53 (1977); Y. C. Tang, M. LeMere, and D. R. Thompson, Phys. Rep. **47**, 167 (1978).
[61] G. D. Alkhazov, A. V. Dobrovolsky, P. Egelhof, H. Geissel, H. Irnich, A. V. Khanzadeev, G. A. Korolev, A. A. Lobodenko, G. Münzenberg, M. Mutterer, S. R. Neumaier, W. Schwab, D. M. Seliverstov, T. Suzuki, and A. A. Vorobyov, Nucl. Phys. A **712**, 269 (2002).
[62] V. V. Burov and V. K. Lukyanov, Preprint JINR, R4-11098, Dubna 1977; V. V. Burov, D. N. Kadrev, V. K. Lukyanov, and Yu. S. Pol', Phys. At. Nucl. **61**, 525 (1998).